JOURNAL OF CATALYSIS 124, 401–415 (1990)

Hydrocarbon Synthesis from CO Hydrogenation over Pd Supported on SAPO Molecular Sieves

R. THOMSON,* C. MONTES,† M. E. DAVIS,† AND E. E. WOLF,*,[1]

*Department of Chemical Engineering, University of Notre Dame, Notre Dame, Indiana 46556; and
†Department of Chemical Engineering, Virginia Polytechnic Institute and State University, Blacksburg, Virginia 24061

Received April 4, 1989; revised version received February 22, 1990

Palladium impregnated on silicoaluminophosphate molecular sieves (SAPO-5, SAPO-11, SAPO-34) and alumina has been studied during CO hydrogenation. Pd/SAPO-5, which exhibited the highest turnover frequencies, initially produced only methane and oxygenates (methanol and dimethyl ether), but catalyzed significant C_{2+} hydrocarbon formation under the same conditions after temporary increase in gas contact time or exposure to propylene. While high yields of C_2–C_4 alkanes were observed over Pd/SAPO-34, reaction over Pd/SAPO-11 and Pd/Al_2O_3 yielded only oxygenates. Methane yields increased significantly with higher temperature, particularly over Pd/SAPO-5. Higher H_2 partial pressures increased oxygenate production and decreased C_{2+} fractions. Many similarities between the results of this work and findings from studies of Pd/ZSM-5 indicate that hydrocarbon synthesis over Pd/SAPO catalysts occurs via a bifunctional pathway, involving methanol synthesis on Pd and autocatalytic conversion of oxygenates responsible for C_{2+} hydrocarbons on the SAPO molecular sieves. Differences in the product distributions from Pd-impregnated molecular sieves arise mainly from the effect of acidity and shape selectivity in methanol conversion on the SAPO molecular sieves.

INTRODUCTION

Conversion of CO/H_2 to methanol has been shown to take place on supported Pd catalysts (*1*). Methanol can in turn be converted to gasoline on ZSM-5 zeolites via the MTG process developed by Mobil (*2*). In a recent work, we have reported the direct conversion of syngas (H_2/CO) to hydrocarbon products on bifunctional catalysts consisting of a methanol synthesis function, Pd, supported on ZSM-5 zeolites (*3*). The reaction pathway was reported to involve CO hydrogenation to methanol on Pd followed by zeolite-catalyzed conversion of methanol to hydrocarbons. The product distribution was strongly dependent on the choice of ZSM-5 zeolite, which also affected both overall CO hydrogenation rate and hydrocarbon yields. This finding was not surprising since palladium-catalyzed methanol formation has been found to be quite sensitive to the choice of support and the presence of promoters (*1*). The extent to which the zeolite function affected the behavior of Pd/ZSM-5 catalysts suggests that use of other types of molecular sieves will likewise influence both activity and product distribution.

The objective of the work reported in this paper is to establish the behavior of Pd-impregnated silicoaluminophosphate (SAPO) molecular sieves as catalysts for CO hydrogenation, particularly toward the formation of C_{2+} products. The aluminophosphate family of molecular sieves ($AlPO_4 - n$) was discovered by Union Carbide (*4*), and more recently, the silicoaluminophosphate family (SAPO-*n*) was disclosed (*5, 6*). These microporous solids exhibit some properties characteristic of zeolites and also show unusual physicochemical traits ascribable to their unique chemical composition (*7, 8*). The ideal $AlPO_4$-*n* consists of tetrahedra of oxygen surrounding aluminum and phosphorus such that Al/P = 1. Thus the $AlPO_4$ network is neutral. In order to create ion exchange capacity and potential acidity, a

[1] To whom correspondence should be addressed.

0021-9517/90 $3.00

portion of the aluminum and/or phosphorus is substituted by the other elements (*4*). For example, the SAPO-*n* molecular sieves can be considered silicon substitution into hypothetical $AlPO_4$-*n* frameworks. The silicon substitution can be for (i) phosphorus (*9*) and (ii) an aluminophosphate pair (*10*). Substitution mechanism (i) leads to cation exchange capacity while mechanism (ii) does not. Also, mechanism (ii) can not occur alone and must be accompanied by (i). If substitution mechanism (i) is present only, then the framework composition is such that Si + P = Al. Such is the case for SAPO-37 (*9*) (silicoaluminophosphate with the structure of faujasite). Silicoaluminophosphates which contain ion exchange capacity can be converted to their acid forms (*4, 5, 9*) and utilized as solid acid catalysts (*4, 5, 11*). It has been shown that SAPO-*n* molecular sieves exhibit shape selective behavior when converting methanol to hydrocarbons (*11*).

In this work we synthesized and characterized SAPO-34, SAPO-11, and SAPO-5 molecular sieves, with micropore sizes ranging from approximately 4 to 8 Å. The activity of these Pd/SAPO-*n* catalysts was studied during CO hydrogenation to hydrocarbons. Characterization of the SAPO-*n* molecular sieves was carried out via ^{29}Si NMR, X-ray diffraction, Ar adsorption, ammonia TPD, and SEM. CO chemisorption was used to determine Pd crystallite size. The activity of each catalyst was studied during CO hydrogenation under various conditions to establish trends of overall activity and selectivity. The catalytic trends were then related to the catalytic properties of the molecular sieves. Comparison of reaction studies of this work with those of Pd/ZSM-5 are made to evaluate the effects of acid functions of different strengths on hydrocarbon yield.

EXPERIMENTAL METHODS

Catalyst preparation. The molecular sieves SAPO-5, SAPO-11, and SAPO-34 were synthesized according to the procedures outlined in Examples 12, 18, and 35, respectively, of the Union Carbide patent (*12*). Here, we substituted pseudoboehmite alumina (Catapal-B) for aluminum isopropoxide in all preparations. HZSM-5 (SiO_2/Al_2O_3 = 68) was provided by the Amoco Research Center and is the same sample as that used previously (*3*).

Prior to metal deposition, the acid forms of the molecular sieves were generated by calcination at 600°C in O_2. Palladium was deposited on the SAPO-*n* solids by the wet impregnation technique reported previously (*3*). Each molecular sieve was slurried in methylene chloride which contained palladium acetylacetone ($Pd(acac)_2$]. The slurry was agitated at room temperature for 24 h, followed by solvent removal by evacuation. Catalysts pretreatment consisted of calcination in O_2 at 400°C for 3 h, followed by subsequent flushing with helium and reduction in flowing hydrogen at 300°C for 3 h.

Catalyst characterization. Silicon, aluminum, and phosphorus were analyzed by electron microprobe analysis with an Applied Research Laboratories SEMQ electron microprobe. Magic angle spinning ^{29}Si NMR spectra were recorded on a Bruker MSL 300 spectrometer. The ^{29}Si spectra were taken at a frequency of 59.8 MHz and a rotation rate of 3–5 kHz, and the chemical shifts are reported relative to Me_4Si (TMS). The X-ray powder diffraction pattern of all samples was recorded on a Nicolet I2 automated diffraction system. Phase identification and purity were obtained from the X-ray powder diffraction pattern.

Argon adsorption isotherms were acquired from the acid forms of the molecular sieves (without Pd) at liquid argon temperatures using an Omnisorp 100 analyzer. Samples were activated by heating to 350°C under vacuum overnight. Ammonia temperature-programmed desorption (TPD) experiments were performed on the acid forms of the molecular sieves. The samples were heated from 50 to 550°C at 10°C/min. Evaluation of each sample was repeated

three to four times to assure reproducible results. Scanning electron micrographs (SEMs) of the SAPO-*n* samples were obtained using JEOL JSM T 300 scanning electron microscope.

Carbon monoxide chemisorption experiments were carried out on the palladium-containing samples immediately after the pretreatment described above. When the reduction was completed, the sample was heated to 400°C under helium and outgassed for 1 h, followed by rapid cooling to room temperature. Pulses of carbon monoxide were then injected into the flowing helium stream until saturation of the sample was detected by a thermal conductivity cell.

IR spectroscopy was used to determine the nature of the species adsorbed on Pd as well as on the molecular sieves. The spectra was recorded using a Digilab 14C FTIR spectrometer. The catalyst, in the form of a self-supporting wafer, was placed on a stainless-steel cell reactor described elsewhere (*3*), which allowed for *in situ* IR transmission under reaction conditions. The catalyst was reduced in flowing hydrogen, at 300°C, then cooled to 250°C and exposed to reaction gases at 250 psi. IR studies of NH_3 adsorption were also conducted at atmospheric pressure on a glass cell in order to differentiate Brönsted and Lewis sites.

Activity studies. Catalyst activity was evaluated using a conventional fixed-bed microreactor (*3*). After placing the catalyst in the reactor, the sample was outgassed at room temperature for 30 min, followed by the reduction in H_2 at 300°C for 3 h. Catalyst charges varied slightly depending on the density of the catalyst, so that contact time remained about the same (0.18 s) throughout the entire study. All kinetic data was taken at a total pressure of 18.0 atm and a flow rate of about 60 sccm. Analysis of the effluent streams was performed by gas chromatography using capillary and Porapak columns (*3*). Oxygen from the oxygenates was rejected as water.

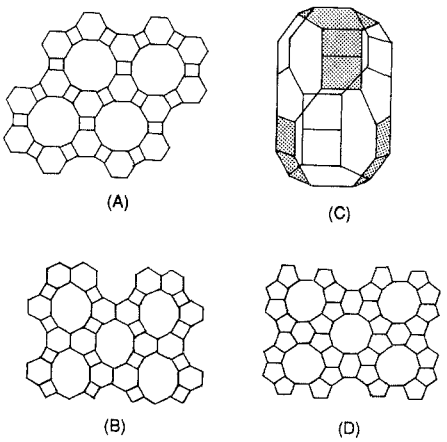

FIG. 1. (A) Framework [001] projection of SAPO-5 and (B) [100] framework projection of SAPO-11; (C) the cage structure of SAPO-34; and (D) [010] framework projection of ZSM-5.

RESULTS

Catalyst characterization. Figure 1 shows the [100] framework projection of SAPO-11, the [001] framework projection of SAPO-5, the [010] framework projection of ZSM-5, and a representation of the "cage" structure of SAPO-34 (analog of zeolite chabazite). SAPO-11 and SAPO-5 contain one-dimensional channels which are elliptical (6.3 by 3.9 Å) and circular (7.3 Å), respectively (*13*). SAPO-34 consists of cages (20-hedron) which are 11 by 6.5 Å with access via pores which are eight-membered rings and have free diameters of approximately 3.9 Å (there could be some variability in this value since the pore size of chabazite is known to change due to the considerable flexibility in the framework (*14*)). ZSM-5 contains straight (5.6 by 5.3 Å) and sinusoidal (5.5 by 5.1 Å) channels which intersect. Thus, in contrast to SAPO-5 and SAPO-11 which contain one-dimensional channels, ZSM-5 and SAPO-34 have multidimensional pore systems.

The chemical compositions of the molecular sieves used in this study are listed in Table 1. The data shown for the SAPOs compare well with the compositions reported by Union Carbide (*12*). Table 1 lists

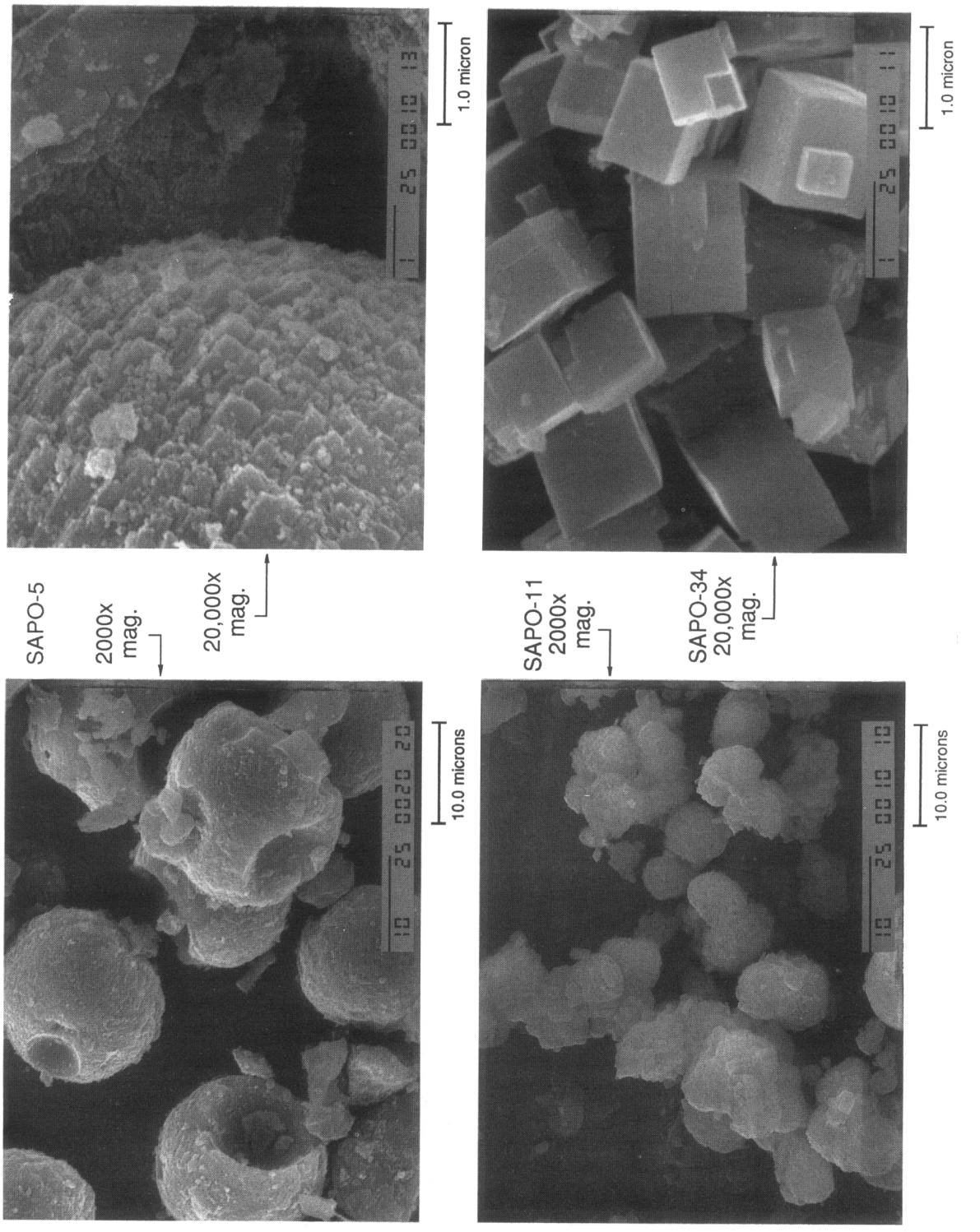
SAPO-5
2000x mag.
20,000x mag.
10.0 microns
1.0 micron
SAPO-11 2000x mag.
SAPO-34 20,000x mag.
10.0 microns
1.0 micron

TABLE 1

Characteristics of Molecular Sieves in Their Acid Forms

Sample	Oxide composition	Total NH_3 desorption (meq/g)	Maximum exchange capacity (meq/g)
HZSM-5	$(Si_{0.972}Al_{0.028})O_2$	0.51	0.47
SAPO-5	$(Si_{0.05}Al_{0.50}P_{0.45})O_2$	0.61	0.82
SAPO-11	$(Si_{0.06}Al_{0.49}P_{0.45})O_2$	0.56	0.99
SAPO-34	$(Si_{0.09}Al_{0.52}P_{0.39})O_2$	1.57	1.48

also the theoretical maximum exchange capacity which is calculated on SAPOs by assuming that each silicon atom equals one exchange site (implying all silicon substitutes for phosphorus) and that on HZSM-5 each aluminum atom equals one exchange site.

Figure 2 shows scanning electron micrographs of the SAPO samples. Note the wide variation in particle morphology; SAPO-34 exhibits a cubic morphology, SAPO-5 appears as spheres composed of small rectangles wrapped around a central cavity, and the SAPO-11 appears as irregular spheroids. The SEM micrographs of ZSM-5, reported elsewhere (*3*), show that their morphology is a function of the degree of crystallinity, and they have a roughly spherical shape.

Figure 3 illustrates the ^{29}Si NMR spectra for the SAPO samples. These results were obtained on samples in their as-synthesized form. Each spectrum contains a major resonance at −90 to −93 ppm with a shoulder at around −110 ppm. For SAPO-11 the intensity of the shoulder is greater than those observed for SAPO-5 and for SAPO-34.

The argon adsorption isotherms of the molecular sieves for $P/P_0 \leq 0.3$, shown in Fig. 4, have the characteristic s-shaped curvature typical for microporous materials.

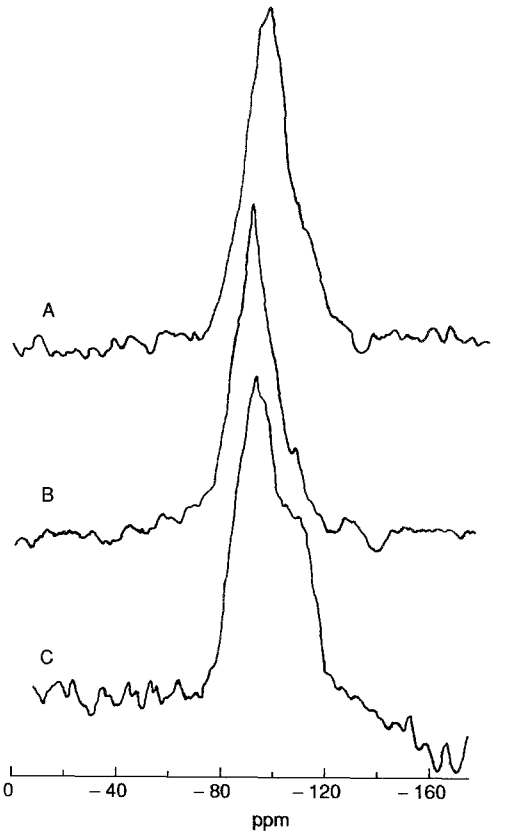

FIG. 3. ^{29}Si NMR spectra of SAPOs. (A) SAPO-5, (B) SAPO-34, and (C) SAPO-11.

SAPO-5, with a 12-member ring channel, clearly shows a higher P/P_0 for the initial transition as expected (curve A). SAPO-11 and ZSM-5 give approximately the same first P/P_0 transition (curves B and D, respectively), which is expected since both have 10-member ring channel systems. The transition for SAPO-34 (curve C) with a smaller pore size occurs between those of SAPO-5 and SAPO-11, which is surprising. Although not shown, the total adsorption capacity of each sample compares favorably to those reported elsewhere (*12, 15*).

The NH_3 TPD spectra of the molecular

FIG. 2. Scanning electron micrographs of SAPOs; (A) and (B) SAPO-5 at two different magnifications; (C) SAPO-11; (D) SAPO-34.

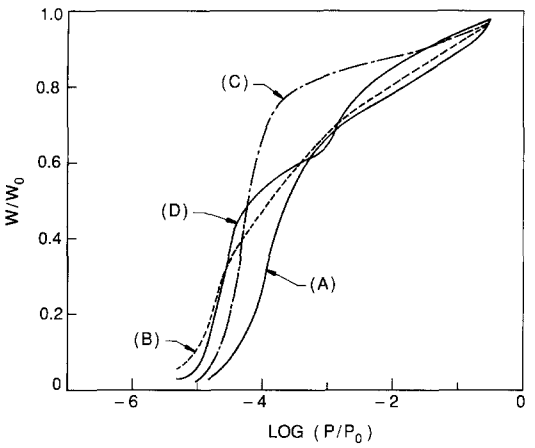

FIG. 4. Argon adsorption isotherms for the molecular sieves. (A) SAPO-5, (B) SAPO-11, (C) SAPO-34, (D) HZSM-5.

sieves without Pd are shown in Fig. 5. ZSM-5 and SAPO-34 both exhibit a low- and a high-temperature desorption peak, whereas SAPO-5 and SAPO-11 show only the low-temperature desorption peak. In Table 1, the total amount of NH_3 desorbed (total area beneath curves given in Fig. 5) from each sample is listed. The SAPO-34 exhibited the highest NH_3 desorption capacity followed by SAPO-5, SAPO-11, and HZSM-5. IR spectra of ammonia adsorbed on the SAPO-*n* molecular sieves after evacuation showed the presence of a band at 3400–3600 cm^{-1} only on HZSM-5 and SAPO-34. This band can then be associated with the high-temperature NH_3 desorption peak exhibited by these catalysts.

CO chemisorption results on the Pd/SAPO-*n* catalysts are summarized in Table 2. The corresponding palladium average crystallite size was calculated from these measurements assuming a 7.9 $Å^2$ area per Pd atom. The average size of the Pd crystallites, ranged from 33–131 Å, which is well above the pore sizes of the molecular sieves. Consequently the majority of the palladium particles is likely to be on the exterior surfaces of the molecular sieve crystals.

TABLE 2

Characteristics of Palladium Crystallites on the Molecular Sieves

Catalyst	Dispersion[a]	Pd crystallite size (Å)[b]
Pd/HZSM-5[c]	0.094	125
Pd/SAPO-5	0.090	131
Pd/SAPO-11	0.210	56
Pd/SAPO-34	0.290	41

[a] Ratio of chemisorbed carbon monoxide to palladium surface atoms taken to be 0.52 (*3*).

[b] Palladium crystallites assumed to be hemispherical, with palladium atoms having a volume of 15.5 $Å^3$.

[c] From Ref. (*3*).

Catalyst activity. Steady-state CO conversion rates for each catalyst are listed in Table 3. The CO conversion in all runs was kept below 5% so that the reported rates were obtained under *differential* conditions. Large differences in overall CO hydrogenation rates were not observed on the different SAPO-*n* molecular sieves. However, when Pd dispersion is accounted for

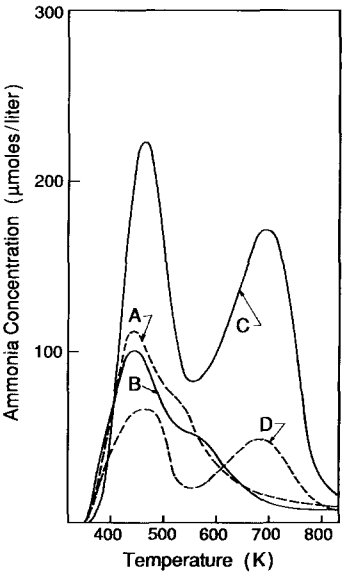

FIG. 5. NH_3 TPD spectra for the molecular sieves. (A) SAPO-5, (B) SAPO-11, (C) SAPO-34, (D) HZSM-5.

TABLE 3

Steady-State Activity

Catalyst	Activity $\times 10^6$ (mol CO conv/gcat-min)	Turnover frequency $\times 10^3$ (molecules/site-s)	Activation energy (Kcal/mole)
2% Pd/SAPO-5	21.1	20.7	15.2
2% Pd/SAPO-11	21.8	9.2	14.9
2% Pd/SAPO-34	15.6	4.8	17.9
2% Pd/Al_2O_3	23.4	5.8	14.3
2% Pd/HZSM-5[a]	3.5	3.3	18.8

[a] From Ref. (*3*).

using CO chemisorption results, Pd/SAPO-5 is seen to have a higher turnover frequency.

The selectivity of Pd/SAPO-5 during CO hydrogenation, shown in Fig. 6, changed drastically with catalyst history. Initially, exposure of Pd/SAPO-5 for 17 h to the reaction conditions (T = 523 K, P = 18.0 atm, H_2/CO = 2.0, and flow = 60 sccm, referred to hereafter as standard conditions) yielded methane and oxygenates (methanol and dimethylether), with only traces of C_{2+} hydrocarbons (Fig. 6a). Decreasing the flow rate to 30 sccm led to the formation of C_{2+} products, with selectivities exceeding 70% (Fig. 6b). Return to standard conditions showed, in contrast to the initial exposure, a markedly lower oxygenated fraction and higher yields of C_{2+} hydrocarbons (Fig. 6c). Similar results were obtained by exposing the catalyst to propylene treatment between standard steady states. In this case, the reaction, having reached steady state under the initial conditions, was stopped by decreasing the pressure to 1 atm, followed by switching the feed to pure nitrogen. The catalyst was outgassed at 250°C for 1 h, then treated with 10% C_3H_6 in N_2 for 30 min, followed by another hour-long outgassing period. Resumption of CO hydrogenation under standard conditions showed Pd/SAPO-5 to be much more active for C_{2+} hydrocarbon synthesis. Comparison of steady states after decreased flow rate and after propylene exposure reveals similar product distributions. All further results re-

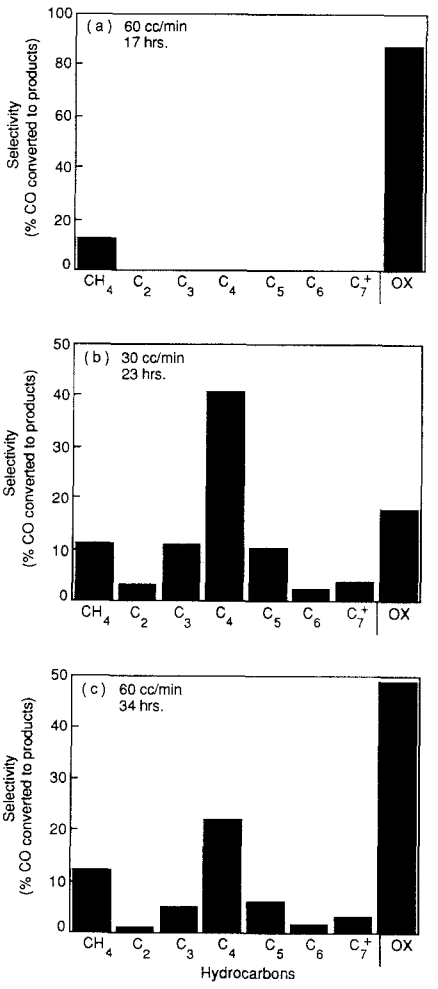

FIG. 6. Effect of flow rate on selectivity over Pd/SAPO-5 at standard steady state (T = 523 K, P = 18.0 atm, H_2/CO = 2.0, flow = 60 sccm/min). (a) Flow rate = 60 sccm/min; time-on-stream = 17 h. (b) Flow rate = 30 sccm/min; time-on-stream = 23 h. (c) Flow rate = 60 sccm/min; time-on-stream, 34 h.

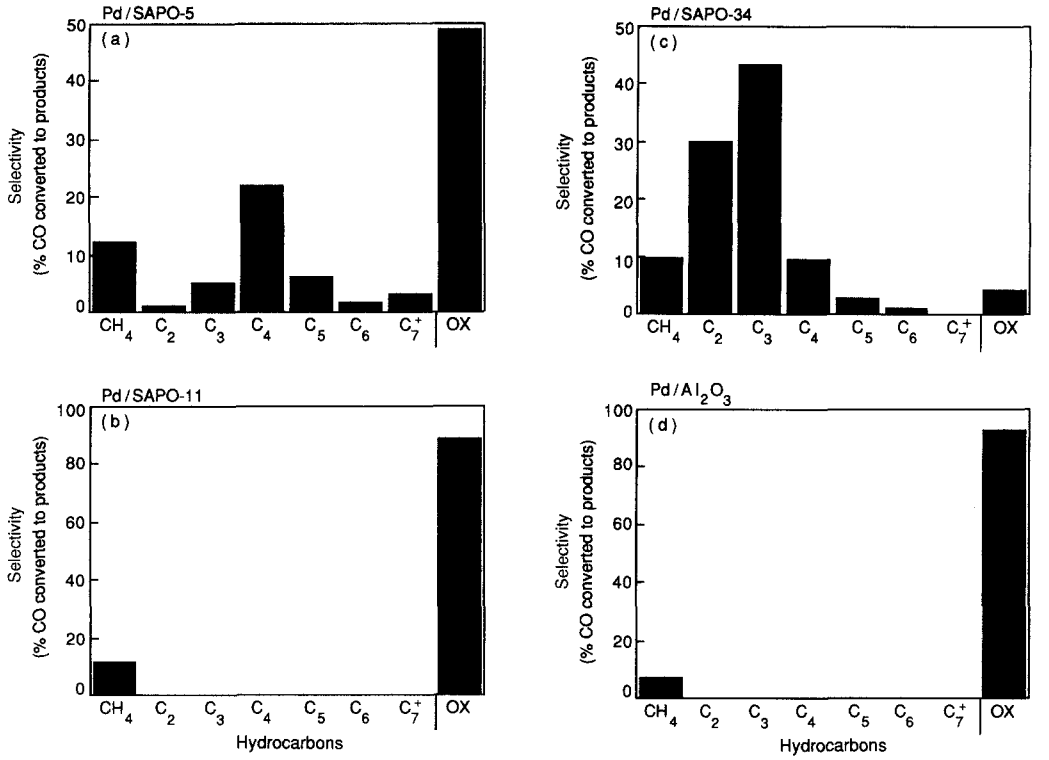

FIG. 7. Product distributions at standard steady state. (a) Pd/SAPO-5; (b) Pd/SAPO-11; (c) Pd/SAPO-34; (d) Pd/Al_2O_3.

ported in this work were taken from Pd/SAPO-5 activated by temporarily decreasing the flow rate.

Selectivities at standard steady state for all catalysts studied are shown in Fig. 7. The results shown in Fig. 7a for Pd/SAPO-5 were obtained under the same conditions as those shown in Fig. 6c. Pd/SAPO-11 (Fig. 7b) and Pd/Al_2O_3 (Fig. 7d) exhibited high selectivity for oxygenates, with the balance consisting of methane. No changes in the product distribution of Pd/SAPO-11 took place when the flow rate was decreased or propylene exposure was employed. In the case of Pd/SAPO-34 (Fig. 7c), however, high selectivities to C_1–C_5 alkanes were detected after only 1 h time-on-stream. During the induction period of Pd/SAPO-34, the rate of CO hydrogenation remained constant, while oxygenate production decreased with a complementary increase in C_{2+} hydrocarbon fraction. All hydrocarbon products obtained on Pd/SAPO-*n* catalysts were alkanes.

CO hydrogenation was also studied using two catalyst beds in series, consisting of Pd/Al_2O_3 followed by SAPO-5 (Fig. 8). The selectivity of the single-bed bifunctional catalyst (Fig. 8a), was quite similar to that obtained with the follow-bed experiment (Fig. 8b), although in this case the hydrocarbons were primarily olefins instead of alkanes. Even for this two-bed system, high selectivity to oxygenated products (DME and MeOH) was observed. Similar results were obtained with a single bed containing a mixture of Pd/Al_2O_3 and SAPO-5 catalysts (Fig. 8c).

Table 4 shows the isoalkane/normal alkane ratios for butane and pentane products obtained at steady state over Pd/SAPO-5 and Pd/SAPO-34 in this study and

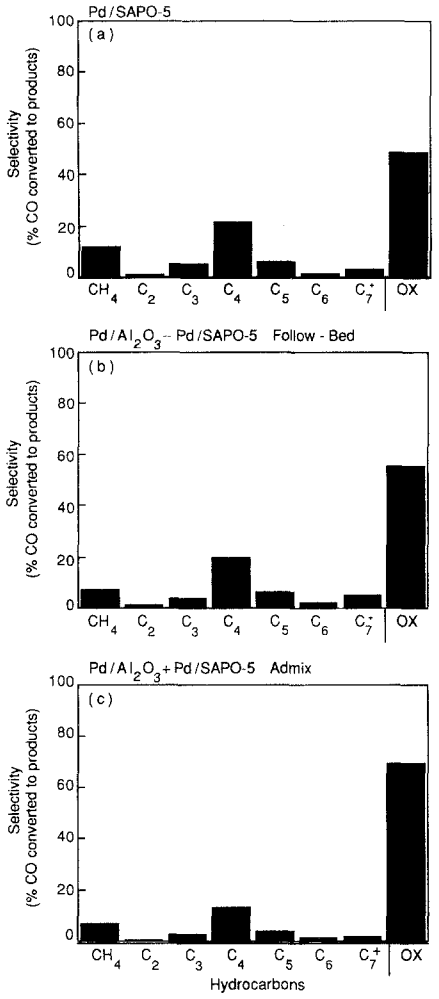

FIG. 8. Selectivities for two beds in series, standard steady state; (a) Pd/SAPO-5, (b) Pd/Al_2O_3 followed by Pd/SAPO-5, (c) Pd/Al_2O_3 + Pd/SAPO admix.

over Pd/HZSM-5 under similar conditions in our previous study (*3*). It is evident that Pd/SAPO-5 produces butanes and pentanes with iso/norm values far exceeding those of Pd/HZSM-5. On Pd/SAPO-34, most of the hydrocarbon products were normal alkanes.

Infrared spectra of Pd/SAPO-5 and Pd/SAPO-34 catalysts under standard reaction conditions, shown in Fig. 9, exhibit absorbance bands similar to those seen for Pd/HZSM-5 (*3*). CO chemisorbed on Pd in a

TABLE 4

Ratio of Iso/Normal Products[a]

Catalyst	iC_4/nC_4	iC_5/nC_5
2% Pd/SAPO-5	6.7	10.8
2% Pd/Al_2O_3–SAPO-5	2.3	>15
2% Pd/SAPO-34	0.0	0.1
2% Pd/HZSM-5[b]	0.9	2.9

[a] Standard reaction conditions.
[b] From Ref (*3*).

bridge-bonded fashion gives rise to the 1970 cm^{-1} band, with an absorbance band due to linear bonding CO masked by the large gas-phase CO band (2200–2000 cm^{-1}). Pd/HZSM-5 showed peaks at 1590 and 1480 cm^{-1}, attributed to formate and methoxy groups, respectively, that existed on the zeolite support (*16*). Bands at 1600, 1480 cm^{-1} on Pd/SAPO-5 and at 1590, 1480 cm^{-1} on

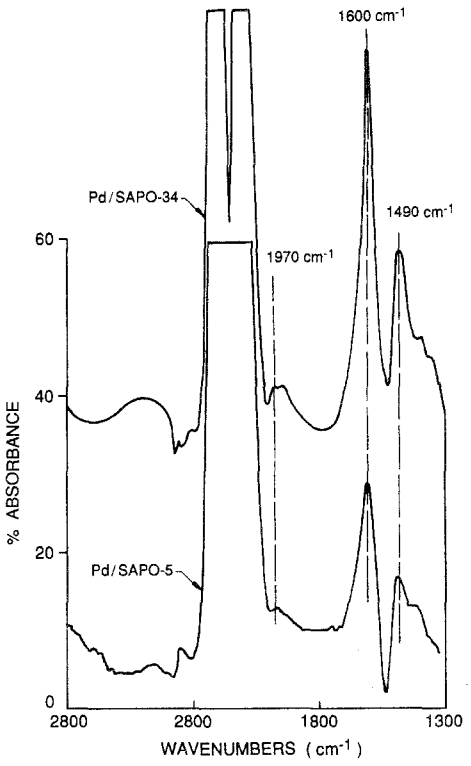

FIG. 9. IR spectra for Pd/SAPO-5 and Pd/SAPO-34 catalysts under standard reaction conditions.

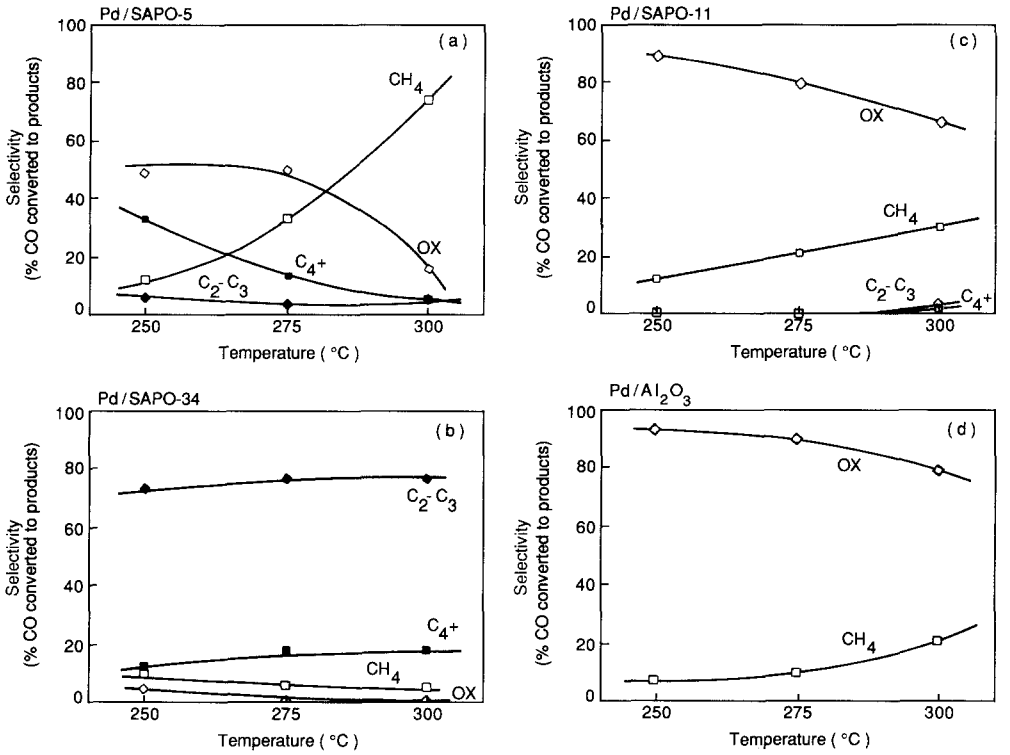

FIG. 10. Effect of temperature on selectivity (P = 18.0 atm, H_2/CO = 2.0, flow = 60 sccm/min); (a) Pd/SAPO-5, (b) Pd/SAPO-34, (c) Pd/SAPO-11, and (d) Pd/Al_2O_3.

Pd/SAPO-34 are similar to those seen on HZSM-5 in this region. The bands for Pd/SAPO-11 (not shown) appear at about the same frequencies as those for the other catalysts, but they are less intense.

After reaching steady state under standard conditions, the catalyst activities were measured at different temperatures (up to 300°C). From the Arrhenius plot, activation energies were found to have values ranging from 14.3 to 17.9 kcal/mole (Table 3), which is a rather narrow range for catalysts exhibiting such different product distributions. Accompanying the expected increase in overall rate with temperature was a significant change in selectivity over three of the catalysts, as seen in Fig. 10. With the exception of Pd/SAPO-34, temperature increases resulted in an increase in the methane selectivity and a decrease in oxygenate selectivity. At the higher temperatures over Pd/SAPO-5, C_{2+} hydrocarbons also decreased to low levels while CH_4 yields neared 80%. The exception to this trend of increasing methane fractions with temperatures was Pd/SAPO-34, with its product distribution relatively insensitive to temperature changes in the range studied.

Variations in the hydrocarbon selectivity were also observed when the ratio of H_2 to CO in the feed was altered (Fig. 11). For both Pd/SAPO-5 and Pd/SAPO-34, increasing the H_2/CO ratio led to higher oxygenate yield while decreasing the C_{2+} hydrocarbon fraction. This trade-off is similar to that observed during the induction period over Pd/SAPO-34. Selectivities over Pd/SAPO-11 and Pd/Al_2O_3 were found to be relatively insensitive to changes in the CO/H_2 feed ratio.

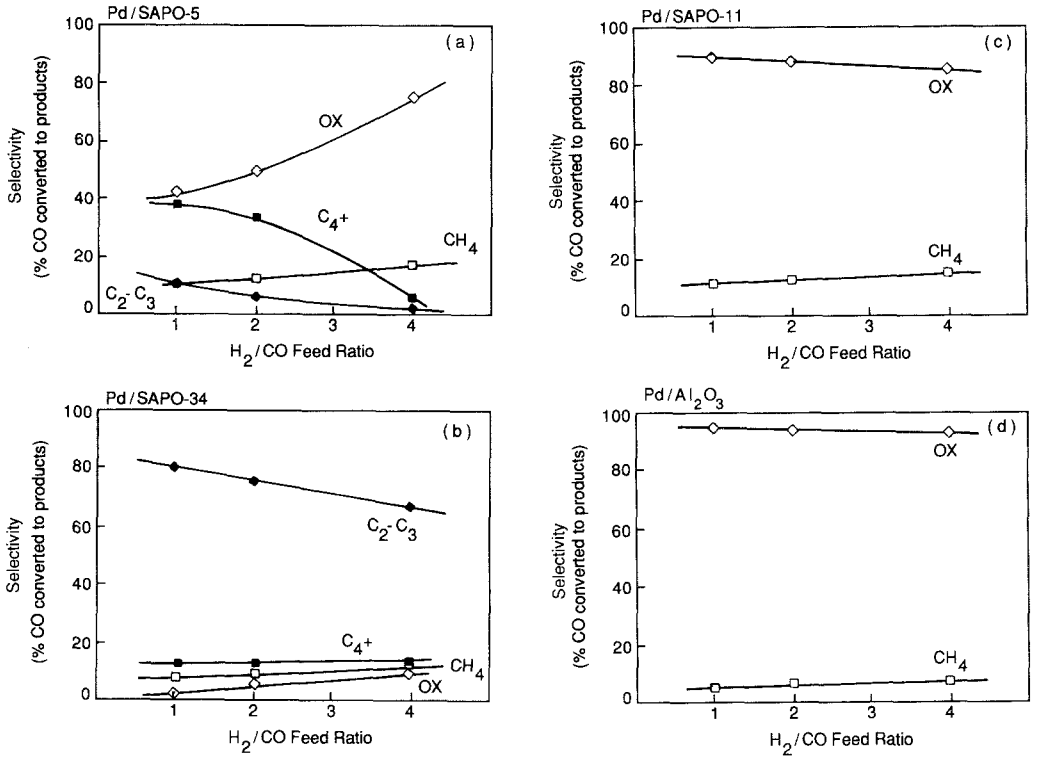

FIG. 11. Selectivities at various H_2/CO feed ratios (T = 523 K, P = 18.0 atm, flow = 60 sccm/min); (a) Pd/SAPO-5, (b) Pd/SAPO-34, (c) Pd/SAPO-11, and (d) Pd/Al_2O_3.

DISCUSSION

Catalyst characterization. The objective of the detailed characterization work carried out was to verify if the synthesis procedures used have yielded the desired SAPO-*n* materials and to determine the nature of Pd dispersion onto the molecular sieves. It remains to clarify from the characterization results the extent of the Si substitution and the properties of these materials.

The argon adsorption isotherms in Fig. 4 show that the materials are microporous. Except for SAPO-34, the molecular sieves exhibit P/P_0 transitions that are in accord with their pore radius (*17*). The higher than expected transition on SAPO-34 could be due to the effect of the cages, the possible flexibility in the chabazite structure, and/or the reaching of the limit of resolution of the technique. For ZSM-5, a second transition around $P/P_0 = 0.001$ is observed. The nature of this phenomenon has been the subject of speculation (*17–19*) and involves adsorbate–adsorbate interactions. Even though the ordering of the P/P_0 transitions does not follow the expected pattern for SAPO-34, the order of magnitude of the transitions is in line with the channel size reported in the literature (*12*).

The chemical compositions (Table 1) and XRD data (not shown) indicate that the synthesis yielded materials that conformed to the specifications of the Union Carbide patent (*12*). The data listed in Table 1 imply that the primary substitution mechanism is silicon for phosphorus (mechanism (i) described earlier). SAPO-5 shows the ideal substitution mechanism (i) (Si + P = Al) while SAPO-11 reveals the presence of

mechanism (ii) as well (Si + P > Al, Al ≠ 0.5). SAPO-34 might contain a slight amount of occluded aluminum, which might explain its high Al content (Al > 5.4 (*4*), although the loss of adsorption capacity is not apparent from the argon sorption studies.

The peak near −90 ppm of the ^{29}Si NMR spectra for the SAPO samples has been assigned to silicon with four aluminum neighbors (via oxygen bridges) resulting from substitution mechanism (i) (*9, 10, 20*). The shoulder at around −110 ppm implies that a single substitution mechanism must not be occurring and that Si–O–Si linkages exist (*10, 20*), and/or small amounts of amorphous silica are present. We do not observe a loss in argon adsorption capacity, which would be expected from the presence of amorphous silica. Thus, we suspect that the intensity around −110 ppm indicates substitution mechanism (ii) for SAPO-5 and SAPO-11. For SAPO-34, the low intensity in the region −100 to −110 ppm would suggest few to no Si–O–Si linkages.

The TPD spectra of NH_3 from the molecular sieves are in good agreement with those published elsewhere for HZSM-5 (*21*), SAPO-5 (*22*), and SAPO-11 (*23*). No data are available for comparison with SAPO-34. Note that SAPO-5 and SAPO-11 show only weak acidity (assumed from temperature maxima in desorption peaks) while SAPO-34 reveals sites with strengths comparable to those of HZSM-5. The total NH_3 desorption from the molecular sieves listed in Table 1 compares extremely well with that of Tapp *et al.* (*23*), who showed that for SAPO-5, with Si/(Al + P + Si) = 0.5, the acid site concentration was less the theoretical maximum calculated by assuming one silicon atom equals one acid site. From the ^{29}Si NMR spectrum of SAPO-5, we expect this result to be true also. The ^{29}Si NMR spectrum of SAPO-11 indicates that its exchange capacity should be well below the theoretical maximum, which agrees with the NH_3 TPD. From the NH_3 desorption, the number of acid sites in SAPO-11 is approximately half of the total number of silicon atoms in the sieve. For HZSM-5 and SAPO-34, which show strong acid sites, the total number of NH_3 molecules desorbed exceeds the theoretical maximum exchange capacity. The excess above the maximum exchange capacity is most likely due to NH_3 adsorption at Lewis acid centers as suggested by Post and van Hooff (*21*). SAPO-5 and SAPO-11 also contain Lewis acidity (*23, 24*). Thus, the total NH_3 desorption capacity for SAPO-5 and SAPO-11 are probably affected by the presence of Lewis acid centers as well.

In summary, the characterization results indicate that we have synthesized SAPO-5, SAPO-11, and SAPO-34 molecular sieves with 12-, 10-, and 8-ring pore systems, respectively. The primary mechanism of Si substitution is (i); however, some substitution via mechanism (ii) occurs also, in particular in SAPO-11. SAPO-34 might contain a slight amount of occluded Al. The Pd-impregnated SAPO-*n* molecular sieves have palladium particles on the exterior surface of the molecular sieve crystals, although the existence of a small fraction of Pd residing within the pores cannot be ruled out.

Activity results. The activation energies for CO conversion, although varying slightly among the various catalysts, are in the same order as that reported for methanol synthesis on Pd (*25, 26*). Differences in turnover numbers agree with reports indicating that methanol synthesis on Pd is affected by the nature of the support (*27*). The nature of this effect is not clear but it can arise from the interaction of the acidic support and the metal or from particle size effects. Since the acidity resides mainly inside the cages, acidity and compositional effects of the external surfaces of the molecular sieves with the Pd particles are probably relatively small. It is then likely that the differences in turnover frequencies are due to particle size effects.

While the role of the Pd function on methanol synthesis is fairly clear, the de-

tailed pathway of oxygenate conversion on the molecular sieves depends on several related factors which are not easy to separate. Experiments with the metal and molecular sieve functions, mixed or used in a follow-bed experiment (Fig. 8), clearly prove that hydrocarbon formation occurs via oxygenate conversion over the SAPO molecular sieves. Although differences are observed in terms of iso and normal products (Table 4) and in the aromatic fraction, the selectivities toward hydrocarbon formation (alkanes) are similar for the Pd/SAPO-5 and Pd/ZSM-5 catalysts. Thus, one can speculate that the conversion of methanol to hydrocarbons follow a similar general reaction pathway on both catalysts. The reaction pathway for hydrocarbon formation on ZSM-5 has been discussed in the literature (*28, 29*). While differences of opinion exist regarding the specific nature of the intermediates, agreement exists about the lumped autocatalytic reaction pathway proposed by Chen and Reagan (*28*) consisting of (1) oxygenates → olefins, (2) olefins + oxygenate → higher olefins, and (3) olefins → aromatics and alkanes. In the bifunctional catalysts, an alternative termination step (4) exists on Pd; olefins + H_2 → alkanes. This model can explain the different product distribution observed in terms of the properties of the molecular sieves. The effect of the H_2/CO ratio and on the product distribution (Fig. 11) agrees well with the above scheme. The autocatalytic step also explains the need for lowering the flow rate or introducing propylene to activate the Pd/SAPO-*n* catalysts.

The Pd/SAPO-5 and Pd/ZSM-5 catalysts are different in terms of their acid strengths, pore size, and pore structure, the former catalysts having one-dimensional 12-ring channels, and the latter having multidimensional 10-ring channels. Since both catalysts have approximately the same Pd dispersion, and assuming no significant support interaction, it follows that CO hydrogenation activity to oxygenates should be nearly the same in both catalysts. However, oxygenate fraction is higher on the Pd/SAPO-5 catalyst; consequently, step 2, leading from oxygenates to higher olefins and step 3, responsible for aromatic formation, must be slower on Pd/SAPO-5. The need to activate the SAPO-5 with propylene or by using longer residence times also supports the argument that the autocatalytic step 2 is slower in this catalyst. The lower acid strength of the SAPO-5 molecular sieve could be responsible for this lower activity of the autocatalytic conversion of oxygenates. The higher iso/normal C_4 and C_5 ratios observed on the Pd/SAPO-5 than on the Pd/ZSM-5 (Table 4) may result from the larger channel size of the SAPO-5, which could accommodate higher concentrations of the iso products than the smaller size channels of ZSM-5.

The lack of hydrocarbon formation on Pd/SAPO-11 is clearly due to the combination of pore size and its one-dimensional channel structure, since it has acidity comparable to that of SAPO-5 and similar IR bands under reaction conditions. The IR bands, although less intense on SAPO-11 than on SAPO-5 (Fig. 9), are indicative that oxygenated species are interacting with the active sites on both molecular sieves (*16*). The band at 1490 cm^{-1} has been ascribed to the methoxy group which has been linked to oxygenate conversion to olefins. The SAPO-11 channel may not accommodate the necessary transition state intermediate for oxygenate conversion, whereas SAPO-5, with larger pore diameter, provides sufficient space for the intermediate and reaction products. Furthermore, the unidimensional structure of the pores on SAPO-11 may have inhibited further the transport of reactants and product in and out of the pores. The Pd/ZSM-5 catalyst has pores of size similar to that of the Pd/SAPO-11 catalyst. However, the multidimensional pore structure of the former has channel intersections where intermediates that are not allowed in a one-dimensional pore can form, and which allows transport in and out of the framework.

The selective formation of light hydrocarbons on Pd/SAPO-34 is similar to results reported for methanol conversion on SAPO-34 to C_3–C_4 hydrocarbons (*11*). The high acid strength, comparable to that of ZSM-5, and the high exchange capacity of SAPO-34 (Fig. 3, Table 1) are probably responsible for the high oxygenate conversion observed in this catalyst (Fig. 7c). The IR spectrum on SAPO-34 is similar to that of SAPO-5 and in fact to that of Pd/HZSM-5 (*3*), indicating that the intermediates associated with the acid functions are the same on these materials. SAPO-34, with a cage structure accessible via eight-membered rings, has micropores smaller (4.3 Å) than those of SAPO-11, yet is capable of hydrocarbon formation whereas the later material is not. This apparent contradiction can be resolved if, in addition to acidity, the pore structure, which in the case of SAPO-34 contain cages versus the one-dimensional SAPO-11, is accounted for. Almost no branched hydrocarbons were observed in the products obtained from SAPO-34 because they cannot diffuse through an eight-membered ring.

Temperature affects CO conversion to oxygenates on Pd and also the other reactions on the molecular sieves. Methane formation increases with temperature in all catalysts except SAPO-34, in agreement with the higher activation energy of the methanation reaction on Pd (*27*). Higher methane production is observed on Pd/SAPO-*n* catalysts than on Pd/Al_2O_3, indicating that methane formation from oxygenates increases as temperature increases. Methane production has also been shown to occur for methanol conversion on ZSM-5 (*28*), in agreement with the previous argument. On Pd/SAPO-34, apparently the drain off of oxygenated intermediates from the Pd surface lowers methane production as temperature increases. The effect of H_2/CO ratio agrees with the trends expected from the reaction pathway, i.e., increasing hydrogen concentration decreases olefin production and thus decreases hydrocarbon formation.

In summary, the results obtained in this work show that CO hydrogenation occurs in all the Pd/SAPO-*n* and on Pd/Al_2O_3 catalysts with similar overall CO conversion rates and activation energies. Hydrocarbon synthesis, however, was highly specific of the molecular sieves used, ranging from no detectable C_{2+} hydrocarbons for Pd/SAPO-11, to a highly selective fraction of C_2 to C_4 hydrocarbon range for Pd/SAPO-34, to a wide range of C_{2+} hydrocarbons for Pd/SAPO-5. The bifunctional reaction pathway to hydrocarbon synthesis consisting of methane, methanol, and dimethylether synthesis over Pd, followed by conversion of the oxygenates to C_{2+} products on the molecular sieves, is similar to that previously reported for Pd/ZSM-5 catalysts. The distribution of the hydrocarbon products is determined by the molecular sieve acidity, pore size, and pore structure.

ACKNOWLEDGMENTS

M.E.D. and C.M. acknowledge the donors of the Petroleum Research Fund, administered by the American Chemical Society, for financial support.

REFERENCES

1. Kikuzuno, Y., Kagami, S., Naito, S., Onoshi, T., and Tamaru, K., *Chem. Lett.* 1249 (1981).
2. Weisz, P. B., in "Advances in Catalysis" (D. D. Eley, P. W. Selwood, and P. B. Weisz, Eds.), Vol. 13, p. 137. Academic Press, San Diego, 1962.
3. Thomson, R. T., and Wolf, E. E., *Appl. Catal.* **41,** 65 (1988).
4. Flanigen, E. M., Patton, R. L., and Wilson, S. T., *Stud. Surf. Sci. Catal.* **37,** 13 (1988).
5. Lok, B. M., Messina, C. A., Patton, R. L., Gajek, R. T., Cannan, R., and Flanigen, E. M., *J. Amer. Chem. Soc.* **106,** 6092 (1984).
6. The suffix "*n*" denotes a specific structure type as given in Ref. (*5*).
7. Pellet, R. J., G. N., and Rabo, J. A., *Stud. Surf. Sci. Catal.* **28,** 843 (1986).
8. Derouane, E. G., Nagy, J. B., Fernandez, C., Gabelica, Z., Laurent, E., and Maljean, P., *Appl. Catal.* **40,** L1 (1988).
9. Sierra de Saldarriaga, L., Saldarriaga, C., and

Davis, M. E., *J. Amer. Chem. Soc.* **106,** 2689 (1987).
10. Hasha, D., Sierra de Saldarriaga, L., Saldarriaga, C., Hathaway, P. E., Cox, D. F., and Davis, M. E., *J. Amer. Chem. Soc.* **110,** 2127 (1988).
11. Kaiser, S. W., U.S. Patent 4,499,327 (1985).
12. Lok, B. M., Messina, C. A., Patton, R. C., Gajek, R. T., Cannan, T. R., and Flanigen, E. M., U.S. Pat. 4,440,871 (1984).
13. Meier, W. M., and Olsen, D. H., "Atlas of Zeolite Structure Type." Butterworths, London, 1987.
14. Mortier, W. J., Pluth, J. J., and Smith, J. V., *Mater. Res. Bull.* **12,** 241 (1979).
15. Olsen, D. H., Haag, W. O., and Lago, R. M., *J. Catal.* **61,** 390 (1980).
16. Greenler, R. G., *J. Chem. Phys.* **37,** 2094 (1962).
17. Venero, A. F., and Chiou, J. N., *MRS Symp. Proc.* **111,** 235 (1988).
18. Jacobs, P. A., Beyer, H. K., and Valyon, J., *Zeolites* **1,** 161 (1981).
19. Muller, U., and Unger, K. K., *Stud. Surf. Sci. Catal.* **39,** 101 (1988).
20. Blackwell, C. S., and Patton, R. L., *J. Phys. Chem.* **92,** 3965 (1988).
21. Post, J. G., and van Hooff, J. H. C., *Zeolites* **4,** 9 (1984).
22. Hedge, S. G. Ratnasamy, P. Kustor, J. M. and Kazensky, V. B., *Zeolites* **8,** 137 (1988).
23. Tapp, N. J., Milestone, N. B., and Bibby, D. M., *Surf. Sci. Catal. Stud.* **37,** 393 (1988).
24. Khouzami, R., Coudurieu, G., Mentzen, B. F., and Vedrine, J. C., *Stud. Surf. Sci. Catal.* **37,** 355 (1988).
25. Poustma, M. L., Eleck, L. F., Ibardia, P. A., Risch, A. P., and Rabo, J. A., *J. Catal.* **52,** 157 (1978).
26. Hicks, R. F., and Bell, A. T., *J. Catal.* **91,** 104 (1985).
27. Sudhakar, C., and Vannice, M. A., *J. Catal.* **95,** 227 (1985).
28. Chen, N. Y. and Reagan, W. J., *J. Catal.* **59,** 123 (1979).
29. Dejaife, P., Vedraine, J. C., Bolis, V., and Derouane, E. G., *J. Catal.* **63,** 331 (1980).